This article was downloaded by: [Siauliu University Library]
On: 17 February 2013, At: 04:40
Publisher: Taylor & Francis
Informa Ltd Registered in England and Wales Registered Number: 1072954
Registered office: Mortimer House, 37-41 Mortimer Street, London W1T 3JH, UK

Molecular Crystals and Liquid Crystals

Publication details, including instructions for authors and subscription information:
http://www.tandfonline.com/loi/gmcl20

Study of Nonlinear Optical and Structural Properties of Organometallic Complexes

Jérôme Luc [a], Jacek Niziol [b], Maciej Śniechowski [c], Bouchta Sahraoui [a], Jean-Luc Fillaut [c] & and Oksana Krupka [a]

[a] POMA-Laboratory of Optical Properties of Materials and Applications, University of Angers, Angers Cedex, France

[b] AGH University of Science and Technology, Kraków, Poland

[c] Chemical Science of Rennes, University of Rennes, Rennes, France

Version of record first published: 31 Aug 2012.

To cite this article: Jérôme Luc , Jacek Niziol , Maciej Śniechowski , Bouchta Sahraoui , Jean-Luc Fillaut & and Oksana Krupka (2008): Study of Nonlinear Optical and Structural Properties of Organometallic Complexes, Molecular Crystals and Liquid Crystals, 485:1, 990-1001

To link to this article: http://dx.doi.org/10.1080/15421400801926099

PLEASE SCROLL DOWN FOR ARTICLE

Full terms and conditions of use: http://www.tandfonline.com/page/terms-and-conditions

This article may be used for research, teaching, and private study purposes. Any substantial or systematic reproduction, redistribution, reselling, loan,

sub-licensing, systematic supply, or distribution in any form to anyone is expressly forbidden.

The publisher does not give any warranty express or implied or make any representation that the contents will be complete or accurate or up to date. The accuracy of any instructions, formulae, and drug doses should be independently verified with primary sources. The publisher shall not be liable for any loss, actions, claims, proceedings, demand, or costs or damages whatsoever or howsoever caused arising directly or indirectly in connection with or arising out of the use of this material.

Downloaded by [Siauliu University Library] at 04:40 17 February 2013

Mol. Cryst. Liq. Cryst., Vol. 485, pp. 242/[990]–253/[1001], 2008
Copyright © Taylor & Francis Group, LLC
ISSN: 1542-1406 print/1563-5287 online
DOI: 10.1080/15421400801926099

Taylor & Francis
Taylor & Francis Group

Study of Nonlinear Optical and Structural Properties of Organometallic Complexes

Jérôme Luc[1], Jacek Niziol[2], Maciej Śniechowski[3], Bouchta Sahraoui[1], Jean-Luc Fillaut[3], and Oksana Krupka[1]
[1]POMA-Laboratory of Optical Properties of Materials and Applications, University of Angers, Angers Cedex, France
[2]AGH University of Science and Technology, Kraków, Poland
[3]Chemical Science of Rennes, University of Rennes, Rennes, France

In the frame of this work, we studied organometallic complexes in form of thin films oriented by corona poling. We report measurements of second and third-order nonlinear optical properties (NLO) obtained by SHG and THG techniques. For each compound studied, we determine the electronic contribution of the effective second and third-order nonlinear susceptibilities. Finally, we use X-ray diffraction to study structure of these compounds, induced by corona poling.

Keywords: corona poling; nonlinear optics; SHG; THG; XRD

Downloaded by [Siauliu University Library] at 04:40 17 February 2013

1. INTRODUCTION

Organometallic materials has received recently considerable attention for possible applications in nonlinear optics and quantum electronics [1]. It was shown that ruthenium derivative chromophores incorporated into the PMMA polymer matrices might be promising materials for optical poling [2].

In this article, we report some results obtained in the NLO characterization of a novel series of donor-acceptor bis-alkynyl ruthenium chromophores used in thin films. First, these thin films were oriented by a corona poling technique and are optically characterized using SHG and THG. Next, X-ray diffraction (XRD) technique was used to

This work was partly supported through research grant no. T08E 083 30 from polish Ministry of Science and Higher Education.

Address correspondence to Jacek Niziol, Faculty of Physics and Applied Comuter Science, AGH University of Science and Technololgy, al. Mickiewicza 30, Kraków, 30-059, Poland. E-mail: gjniziol@cyf-kr.edu.pl

correlate NLO properties and directly observed microscopic order of the studied materials.

2. MATERIALS

2.1. Organometallic Complexes

The syntheses of alkynyl complexes (*trans*-[Ru(4-C≡CC_6H_4N=NC_6H_4-N(C_4H_9)$_2$)Cl(dppe)$_2$] (**A**); *trans*-[Ru(4-C≡CC_6H_4N=NC_6H_4-N(C_4H_9)$_2$)(4-C≡CC_6H_4CHO)(dppe)$_2$] (**B**); and *trans*-[Ru(4-C≡CC_6H_4N=NC_6H_4-N(C_4H_9)$_2$)(4-C≡CC_4H_2SCHO)(dppe)$_2$] (**C**)) have been carried out according to previously reported procedures [3]. Bis-alkynyl ruthenium chromophores were asymmetrically functionalized around the ruthenium centre as shown in Figure 1.

The π-conjugated spacer, consisted of an azo and an organometallic bis-alkynyl-ruthenium group, provided a long conjugation between the donor group (N,N-dibutylamine) and three different acceptors. Very important feature of these complexes is their ability to film formation through casting from solution. In the present study, thin films were obtained by spin-coating from dichloromethane solution.

3. MEASUREMENT METHODS

3.1. Theory of Second Harmonic Generation

Comprehensive theory of SHG has been developed in the late sixties by Boyd [4,5]. The NLO coefficients associated with SHG are

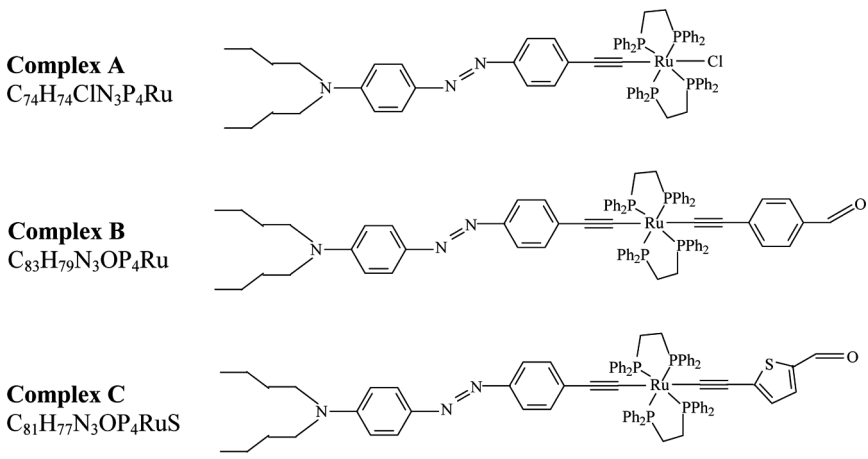

FIGURE 1 Chemical structures of studied organometallic complexes.

Downloaded by [Siauliu University Library] at 04:40 17 February 2013

determined almost exclusively by the Maker fringes technique [6,7]. However, their theory did not consider absorbing materials as in the case of our investigated thin films. Later, Herman and Hayden developed model, which encounters birefringence and absorption [8].

In order to take into account effects of absorption, we write the index of refraction for the nonlinear film as a complex quantity and solve the same boundary-value problem. By writing the complex index of refraction as $\tilde{n}_m = n_m(1 + i\kappa_m)$, where κ_m is the extinction coefficient of the nonlinear material at the frequency $m\omega$ (with $m = 1$ or 2), we receive the following expression for the transmitted SH intensity (neglecting reflections):

$$I_{2\omega}^{(\gamma\to\eta)} = \frac{32\pi^3}{c_0}\frac{(t_{\omega-af}^{\gamma})^4 (t_{2\omega-fs}^{\eta})^2 (t_{2\omega-sa}^{\eta})^2}{n_{2\omega}^2 \cos^2\theta_{2\omega}} \times I_{\omega}^2 \left(\frac{2\pi L}{\lambda_\omega}\right)^2 \left(\chi_{eff}^{\langle 2\rangle}\right)^2 e^{[-2(\delta_1+\delta_2)]} \frac{\sin^2\Psi + \sin\mathrm{h}^2\Omega}{\Psi^2 + \Omega^2} \tag{1}$$

where κ_m is the extinction coeffecient of the nonlinear material at the frequency $m\omega$ (with m = 1 or 2), with:

$$\Psi = (2\pi L/\lambda_\omega)(n_\omega \cos\theta_\omega - n_{2\omega}\cos\theta_{2\omega}) \tag{2}$$

$$\Omega = \delta_1 - \delta_2 = (2\pi L/\lambda_\omega)(n_\omega K_\omega/\cos\theta_\omega - n_{2\omega}K_{2\omega}/\cos\theta_{2\omega} \tag{3}$$

where L represents the thickness of thin film, γ the incident polarization (s or p), η the transmitted polarization (s or p), $t_{\omega-af}$ the transmission coefficient for the fundamental wave at the air-film interface. $t_{2\omega-fs}$ and $t_{2\omega-sa}$ represent the transmission coefficients of the second harmonic wave from thin film to substrate and substrate to air, respectively. For a p-polarization of the second harmonic wave and in the case of s-polarization of the fundamental wave (perpendicular to the incidence plane), we obtain:

$$t_{\omega-af} = \frac{2\cos\theta}{\cos\theta + n_\omega \cos\theta_\omega} \tag{4}$$

$$t_{2\omega-fs} = \frac{2n_{2\omega}\cos\theta_{2\omega}}{n_{2\omega}\cos\theta_{2\omega} + n_{2\omega-s}\cos\theta_{2\omega-s}} \tag{5}$$

$$t_{2\omega-sa} = \frac{2n_{2\omega-s}\cos\theta_{2\omega-s}}{n_{2\omega-s}\cos\theta_{2\omega-s} + \cos\theta} \tag{6}$$

Downloaded by [Siauliu University Library] at 04:40 17 February 2013

In the case of *p*-polarization of the fundamental wave (parallel to the incidence plan), we obtain:

$$t_{\omega-af} = \frac{2\cos\theta}{\cos\theta_\omega + n_\omega \cos\theta} \tag{7}$$

$$t_{2\omega-fs} = \frac{2n_{2\omega}\cos\theta_{2\omega}}{n_{2\omega}\cos\theta_{2\omega-s} + n_{2\omega-s}\cos\theta_{2\omega}} \tag{8}$$

$$t_{2\omega-sa} = \frac{2n_{2\omega-s}\cos\theta_{2\omega-s}}{n_{2\omega-s}\cos\theta + \cos\theta_{2\omega-s}} \tag{9}$$

3.2. Theory of Third Harmonic Generation

The THG method is one of the most informative methods for evaluation the electronic contribution to the third-order nonlinear optical susceptibilities. One of the advantages of this technique is that the THG response accounts only for the instantaneous electronic contribution. Indeed, THG is sensitive to ultrafast electronic mechanisms of nonlinear response with attosecond relaxation times, and it is almost insensitive to slower effects, such as electron-vibration relaxation. Generally, third-order nonlinear optical processes involve the use of a fundamental coherent laser beam of sufficient power density. THG describes the process in which a fundamental laser field of frequency ω generates, through nonlinear polarization in the material, a coherent optical field at frequency 3ω. It allows to determine the pure electronic contribution to third-order NLO susceptibility. The other contributions such as thermal, photochromic orientation or other molecular motional contributions, are much slower and therefore automatically separated. The theoretical model used in this work [9] is based on the formalism of the plane waves and the study of the harmonic optical electric fields generated in a nonlinear medium. This model also takes also into account a majority of the parameters which influence the value of $\chi^{\langle 3\rangle}_{elec}$ through the contribution of air and transmission factors on the interfaces of the nonlinear medium.

For the case of a thin film deposited on a glass substrate and placed in ambient conditions, one can obtain for the third harmonic intensity:

$$I^{3\omega} = \frac{64\pi^4}{c^2}\left|\frac{\chi^{\langle 3\rangle}}{\Delta\varepsilon}\right|_s^2 (I^\omega)^3 \left| e^{i(\Psi_s^{3\omega}+\Psi_F^\omega)}[T_1(e^{i\Delta\Psi_s}-1) + \rho e^{i\phi}T_2(1-e^{-i\Delta\Psi_F})] + C_{air}\right|^2 \tag{10}$$

Downloaded by [Siauliu University Library] at 04:40 17 February 2013

with

$$\rho e^{i\phi} = \left[\frac{\chi^{\langle 3\rangle}_{elec}}{\Delta\varepsilon}\right]_F \Big/ \left[\frac{\chi^{\langle 3\rangle}}{\Delta\varepsilon}\right]_s ; \Delta\varepsilon_s = \varepsilon_s^{\omega} - \varepsilon_s^{3\omega} = 7.753 \times 10^{-2}\,\mathrm{F/m}$$
$$\text{and } \Delta\varepsilon_F = \varepsilon_F^{\omega} - \varepsilon_F^{3\omega}$$

The indices S and F correspond to the substrate and film, respectively, t_l^{ω} is the transmission factor of the fundamental wave between air and the thin film and $t_3^{3\omega}$ is the transmission factor of the harmonic wave between the substrate and air. $\Delta\varepsilon_s$ and $\Delta\varepsilon_F$ represent the dispersion of the dielectric constant in the substrate and thin film, $\Delta\Psi_s$ and $\Delta\Psi_F$ are the difference of phase angles in the substrate and thin film, respectively.

The presented transmission factors are defined by:

$$T_t = (t_{12}^{\omega} t_{23}^{\omega})^3 \frac{N_2^{3\omega} + N_2^{\omega}}{N_2^{3\omega} + N_3^{3\omega}} \qquad \text{and} \qquad T_2 = (t_{12}^{\omega})^3 t_{34}^{3\omega} \frac{N_3^{3\omega} + N_3^{\omega}}{N_3^{3\omega} + N_4^{3\omega}} \quad (11)$$

with $N_j^{\omega,3\omega} = n_j^{\omega,3\omega} \cos\theta_j^{\omega,3\omega}$ where $j = 1, 2, 3, 4$. $t_{ij}^{\omega,3\omega}$ represents the transmission factor for the fundamental or harmonic wave between i and j media.

The factor of air compared to vacuum C_{air} is written in the following form:

$$C_{air} = 0.24C' \lfloor t_{23}^{3\omega} t_{34}^{3\omega} e^{i(\psi+\alpha)} - (t_{12}^{\omega} t_{23}^{\omega} t_{34}^{\omega}) e^{-i(\psi+\beta)} \rfloor \text{ with}$$
$$C' = \left[\frac{\chi^{<3>}}{\Delta\varepsilon}\right]_{air} \Big/ \left[\frac{\chi^{<3>}}{\Delta\varepsilon}\right]_s \quad (12)$$

where Ψ is the phase of the air contribution, α the difference of phase on the incident side of sample, and $\beta = \alpha + \Delta\Psi_s$ is the difference of phase on the exit side (between the fundamental and harmonic waves for propagation in air).

3.3. Experimental Setup

The experimental setup used for the SHG and THG measurements was applied in a typical geometry, very often discussed in the literature [10]. The only difference between SHG and THG setups was the selective filter positioned in front of the photodetector measuring the intensity of the harmonic generated by the nonlinear medium. The laser wavelength was 1064 nm from Nd:YAG of pulse duration of 15 ps, average energy of 1.6 mJ per pulse and repetition frequency of 10 Hz. The *p-in* and *p-out* polarizations were used. SHG and THG

Downloaded by [Siauliu University Library] at 04:40 17 February 2013

measurements were performed by rotating the sample through the angular range $\pm 50^\circ$ along an axis that is perpendicular to the beam propagation direction in order to generate Maker-fringe interference patterns. The $\chi_{eff}^{\langle 2 \rangle}$ value of ruthenium complexes was evaluated by comparing the SH signal with that obtained from a *Y-cut* crystal quartz (reference material), using the same conditions. For the silica calibration, we used the value determined recently ($\chi_{elec}^{<3>} = 2.10^{-22} \mathrm{m}^2/\mathrm{V}^2$) [11] which is about two times smaller than previously reported [12]. The refractive indices were not measured by the ellipsometric method. However, for the SHG and THG measurements, we estimated the dispersion of these values by adjusting the theoretical curves on the experimental curves and by considering a constant thickness for the illuminated surface. The thickness of thin films was given with an uncertainty of measurement of ± 10 nm. In this work, the uncertainty of measurement of $\chi_{elec}^{\langle 2 \rangle}$ and $\chi_{elec}^{\langle 3 \rangle}$ is approximately $\pm 10\%$.

Downloaded by [Siauliu University Library] at 04:40 17 February 2013

3.4. SHG-Corona Poling

Thin films made of studied compounds were subjected to corona poling. This technique is commonly used for orienting NLO chromophore confined in optically inert, transparent matrix [13]. We used a home made apparatus, which enabled heating up to 180°C and delivered 12 kV of high voltage. In this work, the optimized parameters to obtain the best second-order nonlinear properties were: 120°C (temperature of corona poling) and 7 kV/mm (electric field) during 5 minutes.

3.5. X-ray Diffractometry

Wide angle X-ray diffraction (WAXS) measurements were carried out in grazing incident beam (GID) reflection geometry using Cu Kα radiation (1.542 Å) and classical Bragg-Brentano [14]. The PanAlytical X'Pert PRO diffractometer was equipped with a parallel beam parabolic Göbel mirror to improve scattering intensities from the film samples. The scan step was 0.1° (in 2θ) with a counting time of 15 s/step. In general, raw data have to be folded with the instrumental resolution of the diffractometer. However in our case, broadening of peaks due to disordering is much larger than those of the instruments. We decided to use all experimental curves as measured just modified by a scaling factor accounting for the differences in size of the samples.

Downloaded by [Siauliu University Library] at 04:40 17 February 2013

4. RESULTS AND DISCUSSION

The UV-VIS-NIR absorption spectra of the investigated ruthenium complexes are shown in Figure 2. The absorption spectra show broad bands with λ_{max} at 498, 488 and 485 nm for **A-C** compounds, which were assigned to a superposition of the π–π^* transition of the azobenzene moieties and of the MLCT (Metal Ligand Charge Transfer) transitions of the alkynyl ruthenium fragments. According to these spectra, absorption of 1064 nm wavelength can be neglected in SHG and THG studies, contrary to their harmonics at 532 and 355 nm. Theory cited above allowed to cope with this inconvenience.

Corona poling induced orientation in all films of **A-C** complexes. An example of SHG pattern before and after corona-poling is shown in Figure 3. Numerical values of $\chi_{eff}^{\langle 2\rangle}$ and $\chi_{elec}^{\langle 3\rangle}$ were derived from SHG and THG measurements and are listed in Tables 1 and 2. In addition data obtained for reference materials (or of well known properties) found using the same experimental stage is cited.

We have found that the value of $\chi_{elec}^{\langle 3\rangle}$ for the compound **B** is the biggest value and the organometallic complexes are approximately 10^2 times greater than the fused silica reference (for the compound **B** $\chi_{elec}^{\langle 3\rangle} = 3 \cdot 10^{-20}\,\mathrm{m^2/V^2}$). This difference may be accounted for the presence of a phenyl-oxygen group in the complex **B** which has the largest conjugation length.

Moreover, the effective second-order nonlinear susceptibility $\chi_{eff}^{\langle 2\rangle}$ of the studied compounds are approximately 10 times smaller than the value of the Y-cut quartz which is the reference material for the SHG measurements. The value of $\chi_{eff}^{\langle 2\rangle}$ for the non-oriented compound **B** is $\chi_{eff}^{\langle 2\rangle} = 0.17\,\mathrm{pm/V}$. After orientation of chromophores by corona poling, the organometallic complexes **A** and **B** preserve the values of $\chi_{elec}^{\langle 3\rangle}$

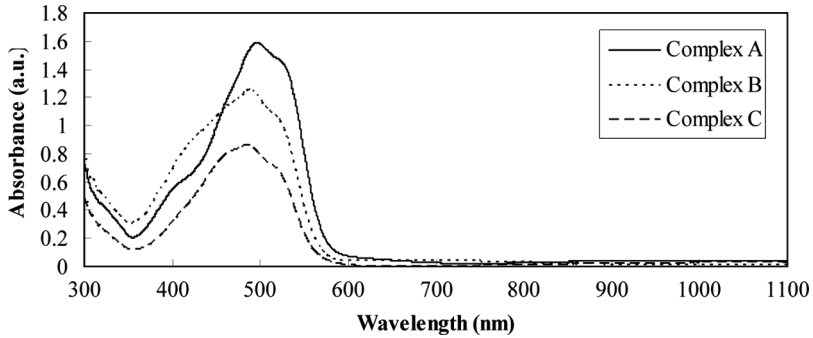

FIGURE 2 UV-VIS-NIR spectra of the studied organometallic complexes.

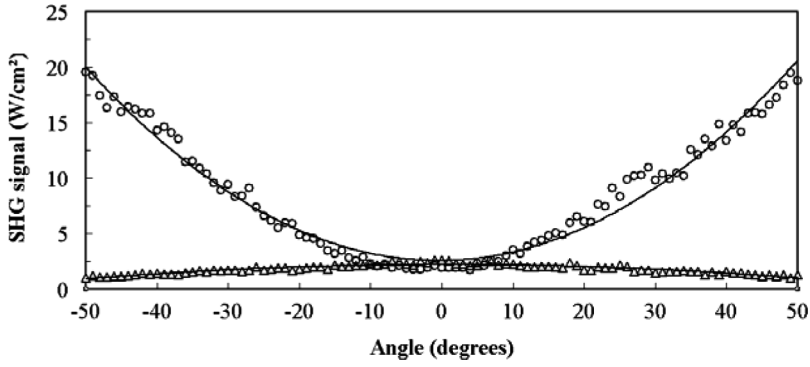

FIGURE 3 SHG-Maker fringes for the complex **B** before (Δ) and after (o) Corona poling (with *pp*-polarization).

and the values of $\chi_{eff}^{\langle 2\rangle}$ are multiplied by two for complex **A** and by six for the complex **B**. Effectively, this difference in the values of $\chi_{eff}^{\langle 2\rangle}$ is due to the longer conjugation length for the complexes **B** and **C** than for complex **A**. In our case, the orientation of chromophores by corona poling allows increasing the second-order nonlinear susceptibility. Moreover, the value of $\chi_{eff}^{\langle 2\rangle}$ for the complex **B** after orientation becomes the same order of magnitude as the value of Y-cut quartz. Principal role here is played by the fact that the doubled frequency signal wavelength is very close [17] to the absorption band shown in the Figure 2.

WAXS diffractograms recorded for of **A**, **B**, **C** complex in powder are shown in Figure 4 and transformed in thin films in Figure 5. Diffractograms obtained for powders indicate differences in crystallinity degree. Powders of **A** and **B** are partly ordered like typical molecular crystals and coherence length is c.a. 300 Å, whilst the sample **C** is virtually amorphous. Once powder were transformed in thin films,

TABLE 1 Thin Film Thicknesses, Second-Order Nonlinear Optical Susceptibility (with *pp*-Polarization), and Third-Order Nonlinear Optical Susceptibility (with *ss*-Polarization) of Studied Compounds

Compounds	Thickness [μm]	$\chi_{eff}^{\langle 2\rangle}$[pm/V]	$\chi_{elec}^{\langle 3\rangle}(\times 10^{-20})[m^2/V^2]$
Fused silica (Ref.) [11]	1010.0	–	0.02
Quartz Y-cut (Ref.) [15,16]	477.0	1.00	–
A	0.2	0.11	1.95
B	0.2	0.17	3.01
C	0.2	0.15	2.72

Downloaded by [Siauliu University Library] at 04:40 17 February 2013

TABLE 2 Comparison (Before and After Corona Poling) of Second-Order Nonlinear Optical Susceptibility (with *pp*-Polarization) and Third-Order Nonlinear Optical Susceptibility (with *ss*-Polarization) for the Complexes **A** and **B** (*for Technical Reasons Thin Film Made of Complex* ***C*** *Didn't Undergo SHG and THG Measurements*)

Compounds	Corona poling	$\chi_{eff}^{\langle 2\rangle}$[pm/V]	$\chi_{elec}^{\langle 3\rangle}(\times 10^{-20})[m^2/V^2]$
A	Before	0.11	1.95
	After	0.23	1.96
B	Before	0.17	3.01
	After	1.02	2.98

Downloaded by [Siauliu University Library] at 04:40 17 February 2013

the order disappeared. First inspection at patterns obtained for films (Fig. 5) revealed only presence of quasi-amorphous peaks. In addition, these diffractograms were virtually identical for all three compounds, thus did not depend on the acceptor subsituent (Cl, benzene, thiophene). The only difference in intensities were due to statistics and film thickness. All these diffraction patterns can be described as consisting of one somewhat sharp reflection at smaller 2θ value ($2\theta = 8.5^{\circ}$), a broader one with an intensity maximum centered at

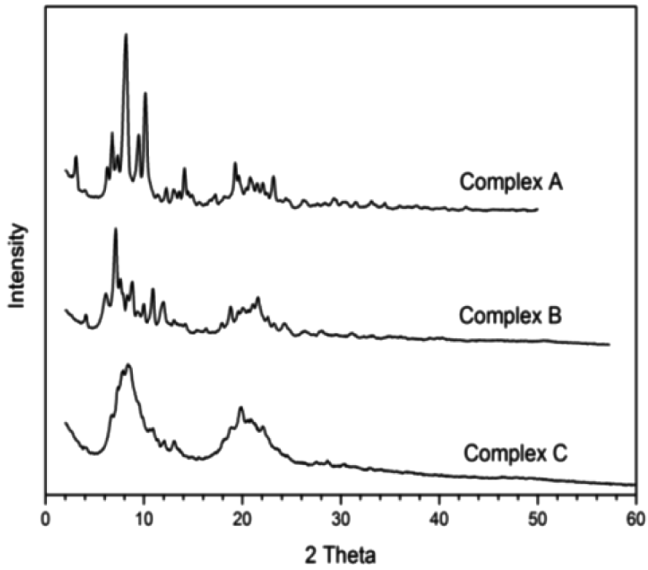

FIGURE 4 WAXS profiles of powders **A**, **B**, **C**. Curves were shifted vertically for clarity.

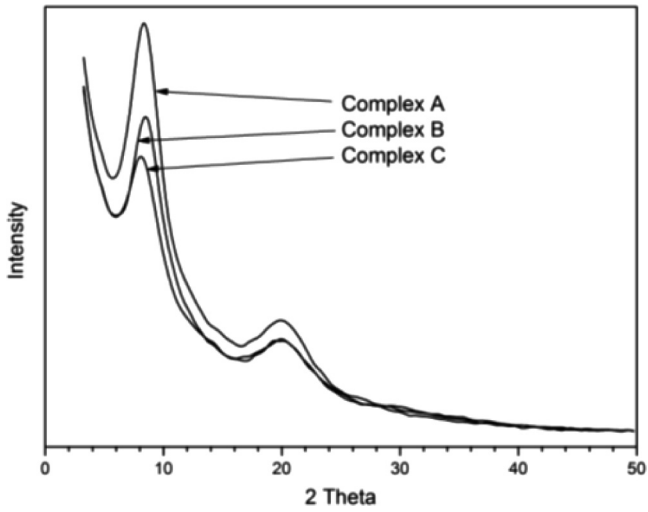

FIGURE 5 WAXS profiles recorded for the thin films **A**, **B**, **C**.

$2\theta = 20^\circ$ both imposed on an exponential background. The positions of these two peaks at $2\theta = 8.5^\circ$ and $2\theta = 20^\circ$, correspond to ordering repeat distances d = 10.5 Å and 4.5 Å respectively. The coherence length (average dimensions of ordered regions) estimated from the broadening of first reflection maxima is around 30 Å - the order is very poor, at distance comparable to the molecule dimensions.

Computation methods of molecular modeling allowed to determine parameters describing this local order. A qualitative comparison of calculated diffractogram according to numerical results and actual measurement data is shown in Figure 6. Both are virtually the same.

We have shown that the treatments of a free standing film with temperature close to glass transition and electric field significantly improve its structural properties. In addition corona poling induces relatively high structural anisotropy of the film. Two dimensional scattering patters were obtained using Eulerian Cradle. Rotation (scanning) of the sample around beam axis, gives direct access to the full range of q vector *(scattering vector)* orientations in respect to film surface. In others words, whole range of crystallography planes present in the sample can be observed (not only those, oriented parallely to the sample substrate). The strong anisotropy is observed between film plane q_xy and scattering vector parallel to the film orientations (Fig. 7). Instead of Debye-like circles (like in polycrystalline samples) well isolated regions of maxima can be

Downloaded by [Siauliu University Library] at 04:40 17 February 2013

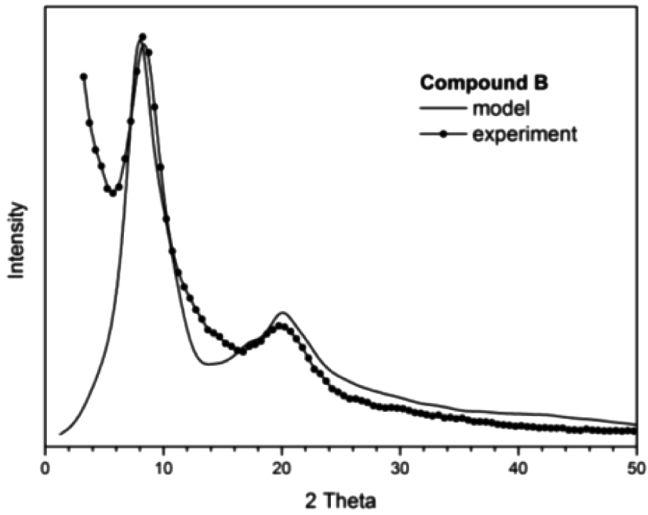

FIGURE 6 Comparison of experimental and simulated WAXS profiles for **B** (experiment-dotted line, model-solid line). Exponent background was not included in computation.

distinguished. This is a finger print of long-range order present in studied samples. Another interesting observation is strong anisotropy of a broad amorphous background. In result of a series of experiment,

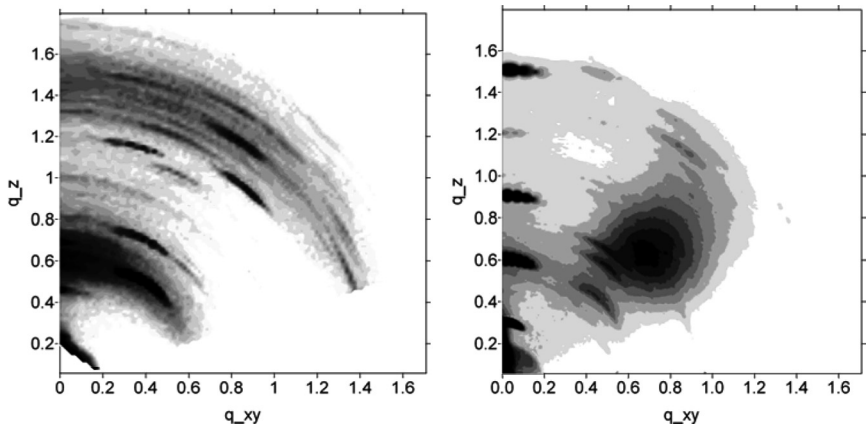

FIGURE 7 2D X-ray scattering paterns of **A** (left) and **B** (right), q_z and q_xy stands for perpendicular to the plane and in-plane components of the scattering vector, respectively.

Downloaded by [Siauliu University Library] at 04:40 17 February 2013

performed under varied conditions, we found that substantial 2D patterns observed for films prepared from compound **A** and **B**, remained similar. Film of **B** was always better oriented than film of **A**, despite the degree of crystallinity invoked by given treatment procedure.

5. CONCLUSIONS

In this paper, we evaluated the electronic contribution, in the picosecond regime, of the effective second and third-order nonlinear optical susceptibilities for a new family of functionalized alkynyl ruthenium complexes. The obtained experimental results well matched the theoretical models. It was also observed that the magnitude of $\chi_{eff}^{\langle 2\rangle}$ correlated with directly observed chromophore crystalline structure induced by corona poling.

Downloaded by [Siauliu University Library] at 04:40 17 February 2013

REFERENCES

[1] Migalska-Zalas, A., Luc, J., Sahraoui, B., & Kityk, I. V. (2006). *Opt. Mat.*, *28*, 1147.
[2] Migalska-Zalas, A., Sofiani, Z., Sahraoui, B., Kityk, I. V., Tkaczyk, S., Yuvshenko, V., Fillaut, J. L., Perruchon, J., & Muller, T. J. J. (2004). *J. Phys. Chem. B*, *108*, 14942.
[3] Fillaut, J.-L., Perruchon, J., Blanchard, P., Roncali, J., Golhen, S., Allain, M., Migalska-Zalas, A., Kityk, I. V., & Sahraoui, B. (2005). *Organometallics*, *24*, 687.
[4] Boyd, G. D., Ashkin, A., Dziedzic, J. M., & Kleinman, D. A. (1965). *Phys. Rev.*, *137*, A1305.
[5] Boyd, G. D. & Kleinman, D. A. (1968). *J. Appl. Phys.*, *39*, 3597.
[6] Maker, P. D., Terhune, R. W., Nisenhoff, M., & Savage, C. M. (1962). *Phys. Rev. Lett.*, *8*, 21.
[7] Kurtz, S. K. & Perry, T. T. (1968). *J. Appl. Phys.*, *39*, 3798.
[8] Herman, W. N. & Hayden, L. M. (1995). *J. Opt. Soc. Am. B*, *12*(3), 416.
[9] Kajzar, F., Messier, J., & Rosilio, C. (1986). *J. Appl. Phys.*, *60*(9), 3040.
[10] Kajzar, F., Agranovich, V. M., & Lee, C.Y.-C. (1996). *Photoactive Organic Materials - Science and Application*, Kluwer.
[11] Bosshard, C., Gubler, U., Kaatz, P., Mazerant, W., & Meier, U. (2000). *Phys. Rev. B*, *61*(16), 10688.
[12] Kajzar, F. & Messier, J. (1985). *Phys. Rev. A.*, *32*(4), 2352.
[13] Kajzar, F. & Chollet, P.-A. (1997). *Poled Polymers and Their Applications to SHG and EO Devices*, Gordon & Breach Science Publishers.
[14] Holy, V., Pietsch, U., & Baumbach, T. (2004). *High Resolution X-Ray Scattering from Thin Films and Multilayers*, Springer, 2nd edition.
[15] Choy, M. & Byer, R. L. (1976). *Phys.Rev. B.*, *14*, 1693.
[16] Kajzar, F., Okada-Shudo, Y., Meritt, C., & Kafafi, Z. (2001). *Synth. Met.*, *117*, 189.
[17] Kityk, I. V., Makowska-Janusik, M., Gondek, E., Krzeminska, L., Danel, A., Plucinski, K. J., Benet, S., & Sahraoui, B. (2004). *J. Phys. Cond. Matter.*, *16*, 231.